A STUDY OF NANOCOMPOSITE WITH NICKEL OXIDE IN TWO AND SIX LINES FERRIHYDRITE

Poonam*

PGT Physics , Kanya Gurukal Sr Sec School Kharal, Narwana, Haryana, India

***Email ID**: poonamduhanmoar@gmail.com*

Accepted: 10.12.2022 **Published**: 01.01.2023

Keywords: Nanocomposite, Nickel Oxide, Two and Six Lines Ferrihydrite, Magnetic Nanoparticles.

Abstract

The role of particle magnetic moment distribution on magnetization of magnetic nanoparticles is used in analysis of magnetization data on a composite of nickel oxide and two lines ferrihydrite nanoparticles in super paramagnetic region. The presented analysis is found to be very helpful in estimating concentration of individual component in a magnetic nanocomposite. Magnetic particles require energy to overcome the energy barrier. This energy can be supplied in form of thermal energy by varying temperature or magnetic energy by varying strength of applied magnetic field. Rate of magnetization relaxation is affected by both temperature and applied magnetic field strength. Magnetization of magnetic nanoparticle systems is also affected by any history. The magnetization relaxation in any system can be nicely studied by measuring magnetization as a function of time at low temperature where the relaxation time is sufficiently large and can be measured easily. But in superparamagnetic state the relaxation time is very small (∼ 10−11 s) and so system achieves equilibrium easily at any temperature and applied magnetic field. In last several decades superparamagnetic behavior of ferro and ferrimagnetic nanoparticles were studied extensively. Researchers showed their interest in these systems mainly because of unique behavior exhibited by them. These systems also have many useful technological applications, as already discussed. But magnetic behavior of antiferromagnetic nanoparticles attracted the attention of scientists mainly in recent decades only.

Paper Identification

**Corresponding Author*

INTRODUCTION

Ferrimagnetism occurs when the adjusting magnetic moments partially cancel. Uncompensated antiferromagnetism is another name for ferrimagnetism. Above Tc, ferrimagnetic materials act like paramagnetic materials and, like ferromagnetic materials, can preserve spontaneous magnetization. Neel pioneered the field of ferrimagnetism by formulating the general theory of the phenomenon. A ferrimagnetic material can have a variety of magnetic properties thanks to the uncompensated sublattice magnetization. Magnetic moments on the two sublattices have different temperature dependences. That's why it's possible for the magnetization to change sign with temperature change. When the sublattice magnetizations just cancel out, the temperature is called Tcomp (thermal comparison point).

It is possible to change the direction of magnetization of a magnetic material by heating it to a temperature greater than the coupling force between atoms in the smaller particles. Magnetic moments are averaged to zero as a result of the variable magnetization. Consequently, the material acts similarly to paramagnetism, except that the moment of the entire particle is aligned with the magnetic field rather than each individual atom being impacted individually by an external magnetic field. Superparamagnetic describes the properties of such particles. Particles with a diameter ranging from 1 to 10 nm exhibit superparamagnetism. Because of the superparamagnetic effect in magnetic data storage, this is especially relevant. Superparamagnetic particles can be used in commercial applications such as magnetic resonance imaging (MRI), RNA fishing, targeted medication delivery, magnetofaction, programmable viscosity (ferrofluid) and high sensitivity sensors.

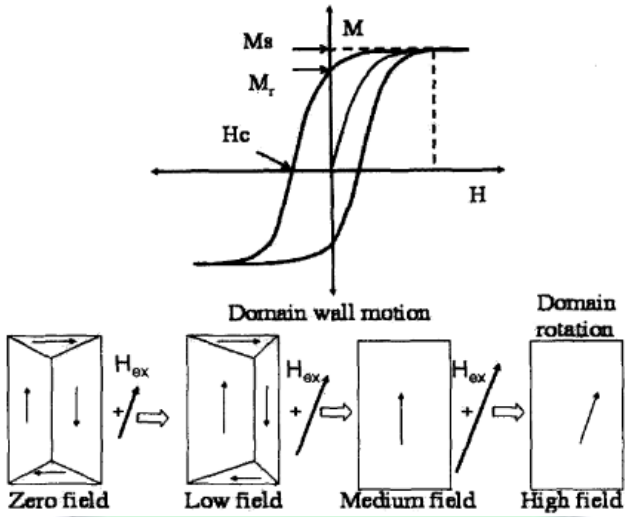

Figure 1: Basic magnetization process in ferromagnetic materials

MAGNETISM IN FERRITES

Uncompensated antiferromagnetism is responsible for the magnetization of ferrites; this is why composition, cation distribution and relative strength of possible interactions all influence magnetization. Due to the enormous cation-cation distances in ferrites, direct exchange interactions are practically nonexistent. In ferrites, the most important contact occurs between octahedral and tetrahedral cations, or A-O-B interactions. The B-O-B superexchange is the next permissible interaction. As a result, the A-O-A interaction does not come into play, as it is extremely weak. Saturation magnetization and Curie temperature are controlled by the strength of exchange contacts, and this exchange interaction is controlled by the distribution of cations. The superexchange interaction is the process through which the magnetic exchange forces between the metal ions in ferrites are mediated by oxygen ions. If there are n identical magnetic ions per unit volume, then a fraction x is situated on the A-sites and a fraction y = (l-x) on the B-sites, respectively. To represent the A and B ion mean moment in the direction of field at temperature T, we have these expressions: (LA, (XB)). Because the ions A and B are identical, but they are exposed to different molecular fields, XA and XA aren't the same.Then the magnetization of the A-sublattice is $M_A = x n \mu_A$. The total magnetization of the two sublattices is

$$M = M_A + M_B \quad (1)$$

The molecular field acting on the sublattice A is

$$H_{mA} = -\gamma_{AB} M_B + \gamma_{AA} M_A \quad (2)$$

and molecular field acting on the sublattice B is

$$H_{mB} = -\gamma_{AB} M_A + \gamma_{BB} M_B \quad (3)$$

The magnetizations of the A and B sublattices, M and MB, are shown in this diagram. IAA, IBB, and JAB represent the strength of the exchange interactions between A-A, B-B, and A-B correspondingly. There are two kinds of interactions occurring here: antiparallel and parallel. The negative sign represents the antiparallel interaction between A and B ions, whereas the positive symbol represents parallel interaction between ions on the same site. Curie's law governs the magnetization of each sublattice.,

$$M_A = \frac{C_A}{T}(H + H_{mA}) \quad (4)$$

$$M_B = \frac{C_B}{T}(H + H_{mB}) \quad (5)$$

Since the Curie constants CA and CB are not identical for the two different sites, the above equations are modified by introducing the term density of ferrimagnetic materials on the right hand sides and now putting the values of HmA and HmB in equations 1.30 and 1.31, the magnetization on the two different sites are obtained as

$$M_A = \frac{\rho C_A}{T}(H + \gamma_{AA} M_A - \gamma_{AB} M_B) \quad (6)$$

And

$$M_B = \frac{\rho C_B}{T}(H + \gamma_{BB} M_B - \gamma_{AB} M_A) \quad (7)$$

After solving these two equations, the mass susceptibility, x> of & ferrimagnetic material is obtained as

$$\chi = \frac{M}{\rho H} = \frac{T}{C} + \frac{1}{\chi_0} - \frac{K}{T - \Theta} \quad (8)$$

where C = CA + CB and K is a constant. Although 0 has the dimension of temperature, it has no physical significance above the Curie temperature. Therefore,

$$\chi = \frac{C}{T - \Theta} \quad (9)$$

As a result of ferrimagnetic materials satisfy the Curie-Weiss law above the Curie temperature. One of the most important magnetic features of CoFe204, CoFe204, is that it has a high saturation magnetization and coercivity. It is one of the most important ferrites in terms of

technical advancement. Even while cobalt ferrite was once thought to be an inverse spinel, new research shows that it is not entirely. Because of its strong coercivity and saturation magnetization, cobalt ferrite has received considerable study. This nanoscale cobalt ferrite is made using a variety of innovative synthetic approaches, including combustion, micro-emulsions, sol-gel syntheses, and more. Among ferrimagnetic spinels, cobalt ferrite has the strongest magnetostriction. Cobalt ferrite's magnetostrictive characteristics were studied in the 1950s on polycrystalline and single crystal materials. Cobalt ferrite has the highest magnetostriction of all ferrimagnetic spinels, both in its single crystal and polycrystalline forms. According to the composition, maximum magnetostriction in single crystals is between 600 and 900 ppm. McCallum et al. recently reported a maximum value close to 230 ppm for polycrystalline cobalt ferrite. Magnetic annealing has been used to increase the magnetostrictive stresses even further. These materials have been proposed as promising for stress sensors. Perovskite Manganites are the subject of this section. In the ideal perovskites type oxides, A-site cations are often larger than B-site cations and are in close proximity to the anions. It is from this mineral, CaTiOs perovskite, that perovskitetype oxides are named. He called it after the eminent Russian mineralogist count Lev Aleksevich Von Perovski who described it in the early 1830s. In 1945, a perovskite oxide, BaTi03, was shown to exhibit ferroelectricity. Many novel ferromagnetic, ferroelectric, and piezoelectric materials were discovered as a result of this finding.The discovery of superconductivity in the perovskite type oxide, $Ba_xLa_{5-x}Cu_5O_{5(3-y)}$ ($x = 1$ and 0.75 and y > 0), and Colossal Magnetoresistance (CMR) in the compound Lao.67Cao.3MnO! (x depends on the oxygen pressure during the synthesis), have caught the attention of many researchers towards this family of materials. It is also interesting to note that the magnetic and electrical properties of these materials can be modified by suitable substitution of proper ions in the perovskite structure.

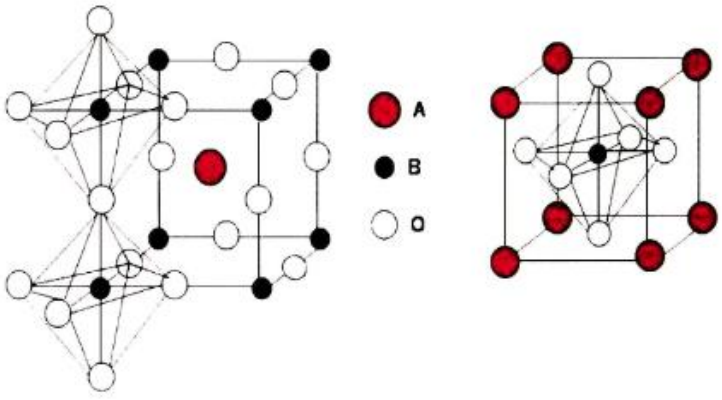

Figure 2: Structural features of an ideal perovskite, ABO3.

STRUCTURAL CHARACTERIZATION

X-ray diffractometers and transmission electron microscopes are used to characterise two lines of ferrihydrite nanoparticles. Figure 3. (a) displays x-ray diffraction results on a powder sample generated at ambient temperature. This figure shows that the dark powder sample is ferrihydrite, which is a single phase with two lines. Estimated lattice-plane separations of 1.50 and 2.24 A are associated with two distinct but parallel diffraction peaks. The broadness of the peaks may be seen in this graph as well. This is an indication of the sample's nanocrystalline nature. X-ray diffraction line broadening and the modified Scherrer formula are used to estimate the average crystallite size. It's around 2 nanometers in diameter. Sample's transmission electron micrograph is depicted in Figure 3.(b). Particles come in a wide variety of forms and sizes, as can be seen in this micrograph. Figure 3 depicts the selected-area electron diffraction pattern from the particles (c). The two peaks in the x-ray diffraction pattern are represented by two rings in this pattern. The arithmetic mean particle size is 2.6 nm, with a standard variation of 0.9 nm. The transmission electron micrograph clearly shows that the mean particle size is close to the average crystallite size measured by x-ray diffraction. Nanoparticles are crystallites by definition.

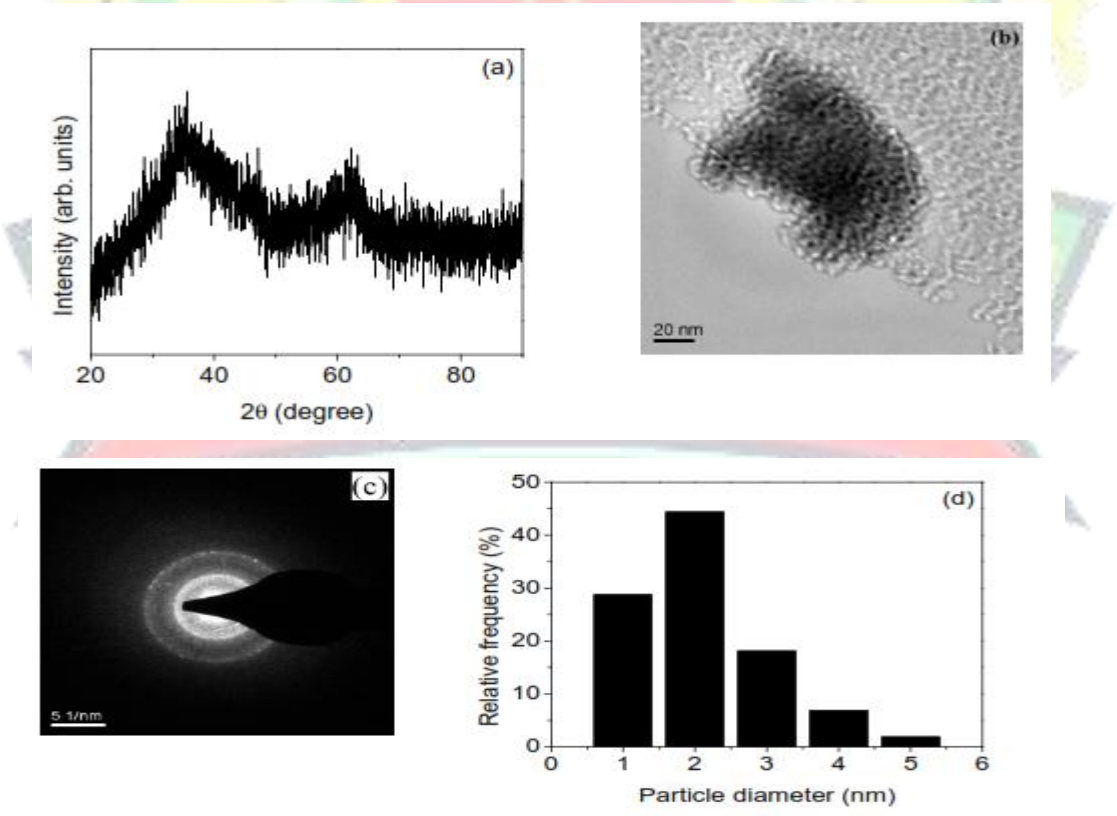

Fig. 3: (a) Room temperature x-ray diffraction pattern of the sample, (b) transmission electron micrograph of the sample, (c) selected area electron diffraction pattern and (d) a histogram of the distribution of particle size.

Figure 3 (d) shows statistical distribution of particle size. This distribution is based on size measurement of 160 particles. It is found to peak at 2 nm.

THERMAL CHARACTERIZATION

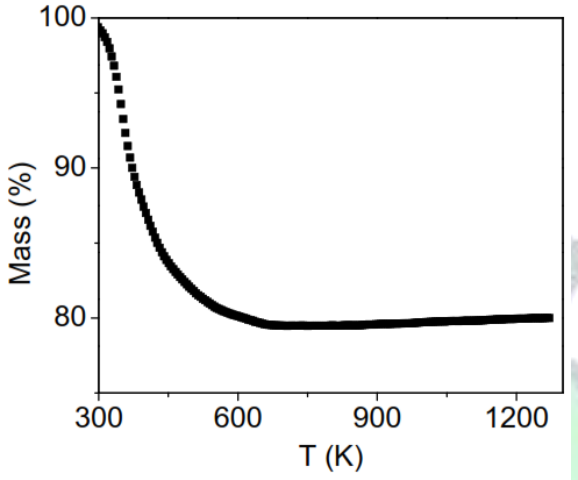

Fig. 4: TGA curve for 2 nm two lines ferrihydrite particles

A thermogravimetric analyser is used to characterise 2 nm two-line ferrihydrite particles (TGA). Figure 4 depicts the sample's TGA curve. An air temperature of 5.0°C per minute is used for the analysis. An increase in temperature causes a drop in mass, although it stabilises about 700 K. At this temperature, the system must be going through a phase change. For three hours, the sample is heated to 873 K in air. A single phase of -Fe2O3 is clearly seen in the pattern. Ferrihydrite nanoparticles dissolve into Fe2O3 when heated, in other words. Diffraction peaks are clearly seen in Fig. 5. It's a sign that the crystallites have grown in size.

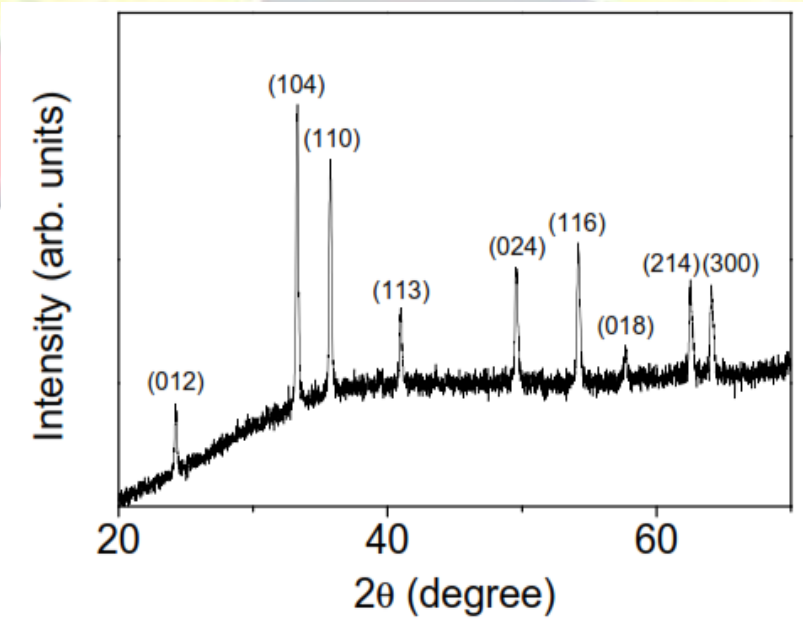

Fig. 5: Room temperature x-ray diffraction pattern of α-Fe2O3.

4.3 MAGNETIC CHARACTERIZATION

1 Temperature dependence

Figure 6 depicts the susceptibility of 2 nm ferrihydrite particles in a 250 G applied magnetic field as a function of temperature T for ZFC and FC in a zero field cooled (ZFC) and field cooled (FC) state. In this graph, we can see that the ZFC susceptibility increases with temperature and reaches its max at 60(5) K. Temperature-dependent decreases in ZFC and FC susceptibility have also been documented. There is further evidence that the ZFC and FC curves split at a specific temperature. A superparamagnetic system has these features. The blocking temperature TB is the temperature at which the ZFC and FC curves split, whereas the bifurcation temperature Tbf is the temperature at which the vs. T curve reaches its apex in zero field cooling. At lower temperatures, the FC susceptibility is shown in Fig. 6 to become nearly temperature independent. A spin glass-like condition at lower temperatures has been blamed for the system's strange behaviour. Particles' magnetic moments are blocked at the bifurcation point. For the current system, TB and Tbf are nearly identical. Above the bifurcation temperature, any magnetic nanoparticle system persists in a superparamagnetic state (SPS)...

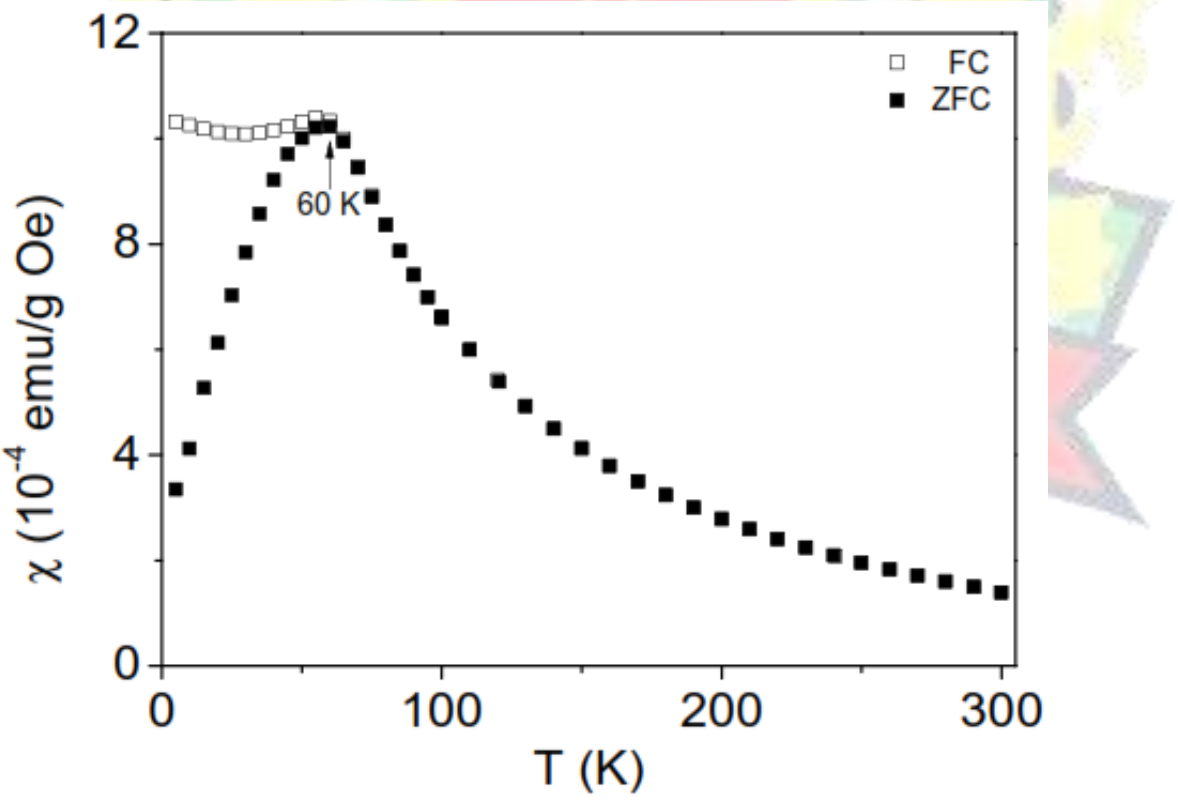

Fig. 6: ZFC (solid symbol) and FC (open symbol) susceptibility χ as a function of temperature T for 2 nm ferrihydrite particles in 250 G applied magnetic field.

2. Field dependence

For 2 nm two lines of ferrihydrite, the M-B loops seen in Figure 7 were observed at 10 and 300 K. At 10 K, there is a hysteresis, whereas at 300 K, there is none. Below Tbf, the system is still stuck in a blocked condition. The M-B loop exhibits hysteresis because the magnetization is not in equilibrium and relaxes very slowly in this state. A superparamagnetic condition is maintained above Tbf. There is no hysteresis in the M-B loop in this state because the relaxation of magnetization is so rapid.

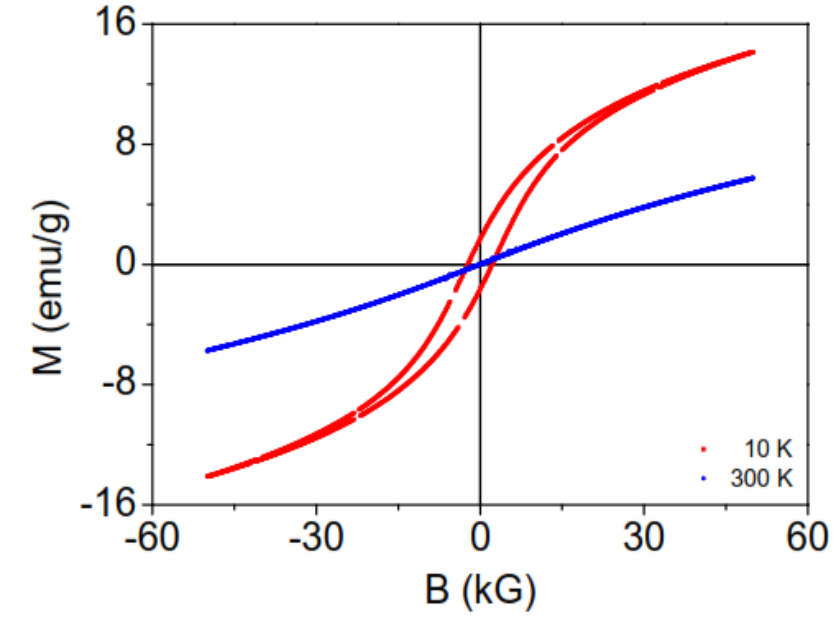

Fig. 7: M-B loops for 2 nm two lines ferrihydrite particles at two different temperatures.

Magnetizations of the 2 nm ferrihydrite particles as a function of applied magnetic field at different temperatures are also measured. Small particles of magnetic materials are likely to be superparamagnetic at sufficiently high temperature.

SIX LINES FERRIHYDRITE

X-ray diffractometer and transmission electron microscope are used to characterise the structural properties of ferrihydrite nanoparticles in six lines. Data from x-ray diffraction on synthetic brown coloured powder is shown in Figure 8 (a). Single-phase six-line ferrihydrite can be deduced from this figure (Fig. 50). Five of the six expected x-ray diffraction peaks can clearly be seen in this figure. Due to finite widening, the last two peaks are quite close to each other and overlap. Five observed diffraction peaks correspond to lattice interplaner spacing values of 1.48, 1.78, 1.97, 2.24, and 2.54 A. The peaks are also shown to be relatively wide in this graph. It is evidence that the sample is nanocrystalline in nature. The modified Scherrer formula is used to calculate the average crystallite size from the widening of the x-ray diffraction line. It's roughly 5 nanometers.

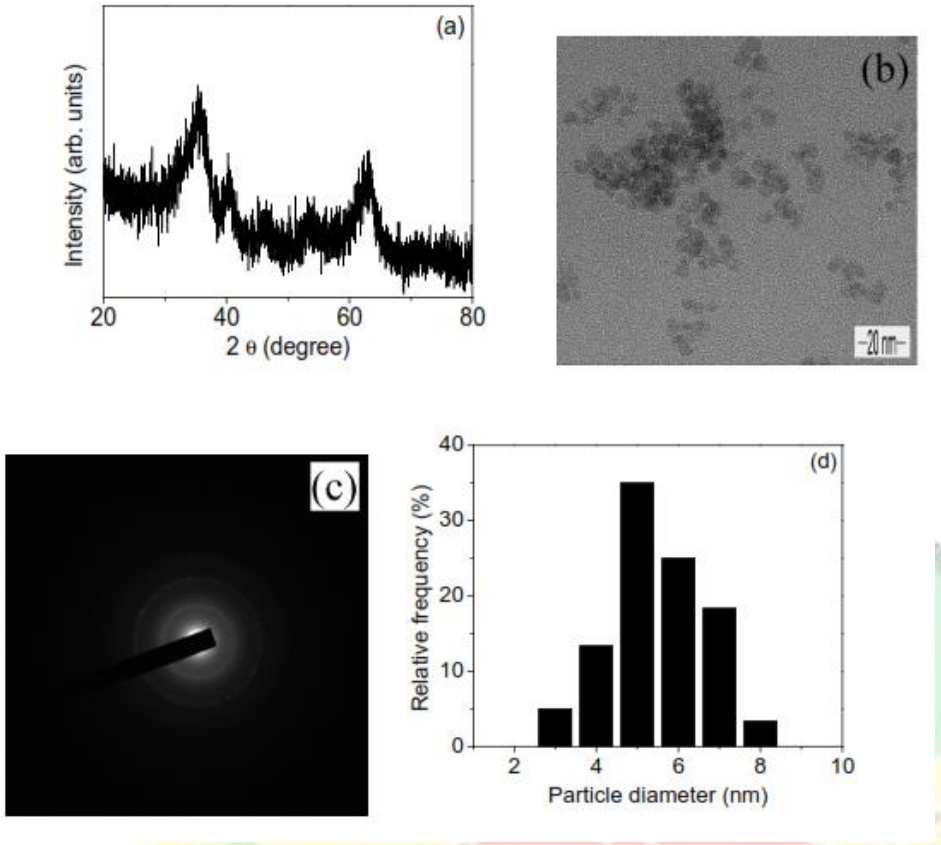

Fig. 8: (a) Room temperature x-ray diffraction pattern of the sample, (b) transmission electron micrograph of the sample, (c) selected area electron diffraction pattern and (d) a histogram of the distribution of particle size.

To visualise the material under electron microscopy, refer to Fig. 8. (b). Particles of all shapes and sizes may be easily seen in this image. in Figure 8, you may see a selected-area electron diffraction pattern from the particles (c). There are only a few faint diffuse rings visible. The arithmetic mean particle size is 5.9 nm, with a standard variation of 1.1 nm, as shown in Fig. 8 (b). The transmission electron micrograph clearly shows that the average particle size is close to the average crystallite size, which was obtained by x-ray diffraction.. As a result, each nanoparticle is, on average, a crystallite. The statistical distribution of particle sizes is shown in Figure 8 (d). The sizes of 160 particles were used to create this distribution. It has been shown to peak at 5 nm.

CONCLUSION

Structure, thermal and magnetic characterizations are provided in this thesis for nanoparticles made of two lines, six lines, and a nickel oxide and two lines ferrihydrite composite. The x-ray diffraction line broadening average crystallite size is comparable to the transmission electron

micrographs average particle size. Each particle is a crystallite, based on this discovery. In addition, transmission electron micrographs indicate that particles can be of any shape or size. Hematite is formed when ferrihydrite nanoparticles are heated in the presence of air. There is a finite size effect that causes all three antiferromagnetic systems studied to display superparamagnetic behaviour. It has been found that zero-field cooled susceptibility increases with increasing temperature, while field cooled susceptibility decreases monotonically. At certain temperatures, both curves bifurcate. Magnetization relaxes slowly below this bifurcation temperature, resulting in hysteresis in the M-B loops. Magnetization relaxes rapidly above the bifurcation temperature, therefore any hysteresis in the M-B loops is absent. Superparamagnetic systems are found in this region. System-specific magnetization data for each system has been analysed thoroughly. The modified Langevin function is used to fit data on the magnetization of two- and six-line ferrihydrite nanoparticles as a function of applied magnetic field. The range of applied magnetic field has been observed to affect the estimated fit parameters. That is, the data does not fit these parameters. Because particle size and shape are not considered in this analysis, there is no consideration given to the distribution of particle magnetic moments. Due to the importance of particle magnetic moment distribution, the magnetization values are adjusted to fit a modified Langevin function. It has been shown that the fit parameters are almost independent of the applied magnetic field range and hence truly define the data. Both forms of ferrihydrite nanoparticles have their magnetization studied at various temperatures in the superparamagnetic zone as a function of the applied magnetic field. In this manner, the distribution of particle magnetic moments in each system can be approximated.

REFERENCES

1. R. W. Chantrell and K. O'Grady, in Applied Magnetism edited by R. Gerber, C. D. Wright, G. Asti (Kluwer Academic Publishers, The Netherlands, 2019).
2. M. Rasa, Eur. Phys. J. E 2, 265 (2020).
3. Q. A. Pankhurst, J. Connolly, S. K. Jones and J. Dobson, J. Phys. D: Appl. Phys. 36, R167 (2018).
4. C. Frandsen, C. W. Ostenfeld, M. Xu, C. S. Jacobsen, L. Keller, K. Lefmann and S. Mørup, Phys. Rev. B 70, 134416 (2019).
5. F. Reif, Fundamentals of Statistical and Thermal Physics (McGraw Hill, Singapore, 1985).

6. S. Jacobs and C. P. Bean, in Magnetism, Vol.III edited by G. T. Rado and H. Suhl (Academic Press Inc., New York, 2018).
7. L. N´eel, in Low Temperature Physics, edited by C. Dewitt, B. Dreyfus and P. D. de Gennes (Gordan and Beach, New York, 2017).
8. S. H. Kilcoyne and R. Cywinski, J. Magn. Magn. Mater. 140-144, 1466 (2015).
9. S. A. Makhlouf, F. T. Parker and A. E. Berkowitz, Phys. Rev. B 55, R14717 (2017).
10. M. S. Seehra, V. S. Babu, A. Manivannan and J. W. Lynn, Phys. Rev. B 61, 3513 (2020).
11. M. S. Seehra and A. Punnoose, Phys. Rev. B 64, 132410 (2016).
12. N. J. O. Silva, V. S. Amaral and L. D. Carlos, Phys. Rev. B 71, 184408 (2015).
13. A. Punnoose, T. Phanthavady, M. S. Seehra, N. Shah and G. P. Huffman, Phys. Rev. B 69, 54425 (2019).
14. R. K¨otitz, W. Weitschies, L. Trahms and W. Semmler, J. Magn. Magn. Mater. 201, 102 (2019).
15. A. Labarta, O. Iglesias, Ll. Balcells and F. Badia, Phys. Rev. B 48, 10241 (2018).
16. G. C. Papaefthymiou, Nano Today 4, 438 (2019).
17. M. M. Ibrahim, S. Darwish and M. S. Seehra, Phys. Rev. B 51, 2955 (2015).
18. L. Neel, Ann. G´eophys. 5, 99 (2019).
19. W. F. Brown, Jr., Phys. Rev. 130, 1677 (2018).
20. S. A. Makhlouf, F. T. Parker, F. E. Spada and A. E. Berkowitz, J. Appl. Phys. 81, 5561 (2017).
21. R. H. Kodama, S. A. Makhlouf and A. E. Berkowitz, Phys. Rev. Lett. 79, 1393 (2017).
22. S. Mørup and C. Frandsen, Phys. Rev. Lett. 92, 217201 (2019).
23. J. T. Richardson, D. I. Yiagas, B. Turk, K. Foster and M. V. Twigg, J. Appl. Phys. 70, 6977 (2016).
24. S. D. Tiwari and K. P. Rajeev, Solid State Commun. 152, 1080 (2017).
25. K. M. Towe and W. F. Bradley, J. Coll. lnterf. Sci. 24, 384 (2017).
26. M. Fleischer, G. Y. Chao and A. Kato, American Mineralogist 60, 485 (2015).
27. J. D. Russell, Clay Minerals 14, 109 (2019).
28. J. Zhao, M. Yang and Z. Hua, J. Magn. Magn. Mater. 371, 10 (2019).